Boundary-layer effects in droplet splashing

Guillaume Riboux* and José Manuel Gordillo†

Área de Mecánica de Fluidos, Departamento de Ingeniería Aeroespacial y Mecánica de Fluidos, Universidad de Sevilla, Avenida de los Descubrimientos s/n 41092, Sevilla, Spain

(Received 22 March 2017; revised manuscript received 19 May 2017; published 13 July 2017)

A drop falling onto a solid substrate will disintegrate into smaller parts when its impact velocity V exceeds the so-called critical velocity for splashing, i.e., when $V > V^*$. Under these circumstances, the very thin liquid sheet, which is ejected tangentially to the solid after the drop touches the substrate, lifts off as a consequence of the aerodynamic forces exerted on it. Subsequently, the growth of capillary instabilities breaks the toroidal rim bordering the ejecta into smaller droplets, violently ejected radially outward, provoking the splash [G. Riboux and J. M. Gordillo, Phys. Rev. Lett. **113**, 024507 (2014)]. In this contribution, the effect of the growth of the boundary layer is included in the splash model presented in Phys. Rev. Lett. **113**, 024507 (2014), obtaining very good agreement between the measured and the predicted values of V^* for wide ranges of liquid and gas material properties, atmospheric pressures, and substrate wettabilities. Our description also modifies the way at when the liquid sheet is first ejected, which can now be determined in a much more straightforward manner than that proposed in Phys. Rev. Lett. **113**, 024507 (2014).

DOI: 10.1103/PhysRevE.96.013105

I. INTRODUCTION

Current technological applications, such as coating, cleaning, cooling, combustion, microfabrication through droplet deposition, or the generation of aerosols, require precise knowledge of the conditions under which a drop hitting a solid substrate either conserves its integrity after the impact, or disintegrates into smaller parts [1]. The relevance of droplet splashing in many natural and engineering processes, and even in forensic sciences [2], together with the advances in high-speed imaging [1], have stimulated the appearance, during the past 20 years, of a vast number of experimental, numerical, and theoretical studies on the subject [3–17]. It is our purpose here to improve the agreement between the critical velocities for splashing predicted by the model presented in [18] and the experimental data. It has been recently reported that the model in [18] (hereafter denoted R&G) is able to quantitatively predict V^*, namely the critical velocity for splashing, in a wide variety of experimental conditions [19–21], this being the reason why we believe that the improvements to the R&G model described here could be useful for researchers working on the description of droplet splashing. Here, we will only refer to the problem of splashing caused by the impact of a drop onto a solid substrate. For information on the analogous physical situation of droplet splashing by impact onto a liquid film, the interested reader is directed to other recent contributions in [22–27].

The starting point of the model proposed by R&G is to determine the ejection time of the lamella T_e, as well as the initial values of the thickness and the velocity of the edge of the liquid sheet, $H_t(T = T_e)$ and $V_t(T = T_e)$ (see Fig. 1). Following R&G, R, V, R/V, and ρV^2 are, respectively, the characteristic length, velocity, time, and pressure used to define the different dimensionless variables, written in lower-case letters to differentiate them from their dimensional counterparts. Here, R indicates the droplet radius, V is the impact velocity, and ρ is the liquid density. Some of the main findings in R&G can be summarized as follows:

(i) The radius of the circular wetted area illustrated in Fig. 1 evolves in time as $a = \sqrt{3t}$ (see R&G).

(ii) The velocity at which the lamella is initially ejected is $v_t(t_e) \simeq \dot{a}(t_e) = 1/2\sqrt{3/t_e}$, with dots denoting time derivatives.

(iii) The thickness of the edge of the lamella at the instant of ejection is $h_t \propto h_a = 2t_e^{3/2}/(\sqrt{3}\pi)$ (see the supplementary material in R&G).

(iv) Since $\dot{a} = v_t$ at $t = t_e$ and the lamella can only be ejected if its tip advances faster than $\dot{a}$, t_e is calculated by imposing that the deceleration of the edge of the lamella, $\dot{v}_t$, coincides with the deceleration of the wetted area, $\ddot{a}$.

In R&G, the ejection time, which is determined by imposing the condition $\dot{v}_t = \ddot{a}$, yields the following equation for t_e:

$$c_1\,\mathrm{Re}^{-1}\,t_e^{-1/2} + \mathrm{Re}^{-2}\,\mathrm{Oh}^{-2} = \ddot{a}h_t^2 = c^2 t_e^{3/2}, \qquad (1)$$

where $\mathrm{Re} = \rho V R/\mu$ and $\mathrm{Oh} = \mu/\sqrt{\rho R\sigma}$ denote, respectively, the impact Reynolds and Ohnesorge numbers, σ is the interfacial tension coefficient, and $c_1 \simeq \sqrt{3}/2$ and $c = 1.1$ are constants adjusted experimentally; the Weber number is defined here as $\mathrm{We} = \rho V^2 R/\sigma = \mathrm{Re}^2\,\mathrm{Oh}^2$. Equation (1) expresses that, in the limit $\mathrm{Oh} \ll 1$, $t_e \propto \mathrm{We}^{-2/3}$, whereas in the moderate to high values of the Ohnesorge number, $t_e \propto \mathrm{Re}^{-1/2}$. We also demonstrate in the supplementary material of R&G that, under the potential flow assumption and for impact velocities such that $V > V^*$, the thickness of the lamella and the liquid velocity at $r = \sqrt{3t}$, i.e., at the radial position where the drop intersects the substrate, are given, respectively, by

$$h_a = 2\,t^{3/2}/(\sqrt{3}\,\pi) \quad \text{and} \quad v_a = \sqrt{3/t}. \qquad (2)$$

Equations (2) were also deduced in [28] in a rather different way from that followed in R&G for the analogous case of the entry of a solid object into a liquid [29–33].

In R&G it is also shown that, once the sheet is ejected, its edge experiences a *vertical* lift force per unit length,

$$F_L = K_l \mu_g V_t + K_u\,\rho_g V_t^2 H_t, \qquad (3)$$

*griboux@us.es
†jgordill@us.es

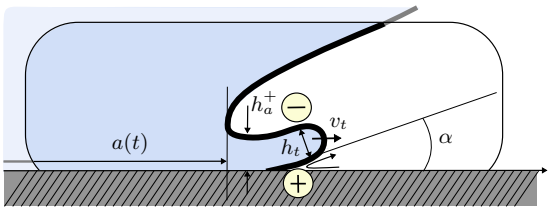

FIG. 1. Sketch of the lamella for $T > T_e$ for $V > V^*$, i.e., for impact velocities above which the lamella dewets the substrate. The regions in which the pressure is larger or smaller than the reference atmospheric pressure are indicated with either a plus or a minus sign. The lift force responsible for droplet splashing results from the integration of the pressure distribution along the edge of the lamella. This figure also illustrates the definitions of the different variables needed to describe the position of the rim.

which results from the addition of the lubrication force exerted by the gas in the wedge region located between the advancing lamella and the substrate (see Fig. 1), $K_l \mu_g V_t$, and the suction force exerted by the gas at the top part of it, $K_u \rho_g V_t^2 H_t$ [18]. Here, the subscript g represents gas quantities, $K_u \simeq 0.3$ is a constant determined numerically, and K_l is deduced using lubrication theory once it is assumed that the front part of the advancing liquid sheet can be approximated to a wedge of constant angle $\alpha \simeq 60^\circ$ while it is in contact with the substrate. The origin of the constant wedge angle α relies on the fact that the no-slip condition provokes the edge of the liquid sheet to be convected further downstream than the region in contact with the solid. This argument is in agreement with the experimental observations in [20], where it was also reported that the substrate wettability does not appreciably affect the splash threshold velocity through α.

The coefficient K_l in (3) is deduced using lubrication theory in the supplementary material of R&G, yielding

$$K_l = -(6/\tan^2\alpha)\{C_2[a\ln(1+a) - a\ln a] + C_3[b\ln(1+b) - b\ln b]\}, \quad (4)$$

with

$$a = 2(\bar{\ell}_g + \bar{\ell}_\mu) + 2\sqrt{(\bar{\ell}_g - \bar{\ell}_\mu)^2 + \bar{\ell}_g\bar{\ell}_\mu},$$
$$b = 2(\bar{\ell}_g + \bar{\ell}_\mu) - 2\sqrt{(\bar{\ell}_g - \bar{\ell}_\mu)^2 + \bar{\ell}_g\bar{\ell}_\mu}. \quad (5)$$

The different coefficients in (4) and the dimensionless variables in (5) are defined as

$$C_1 = \frac{2\,\bar{\ell}_\mu}{a\,b}, \quad C_2 = \frac{1 - C_1\,b}{b - a}, \quad C_3 = -(C_1 + C_2),$$
$$\bar{\ell}_\mu = \ell_\mu/H_0, \quad \text{and} \quad \bar{\ell}_g = \ell_g/H_0. \quad (6)$$

Here, $H_0 = H_t/4$, $\ell_g \simeq 1.2\lambda$ is the slip length of the gas [34], $\lambda = k_B T_g/(\sqrt{2}\pi d^2 p_g)$ is the mean free path between gas molecules, k_B is the Boltzmann constant, T_g and p_g are the gas temperature and pressure, respectively, and d indicates the effective diameter of gas molecules. Values of λ, μ_g, and ρ_g for different gases are provided in Table I. Contrarily to R&G, where $\bar{\ell}_\mu$ in Eq. (5) was set to zero, yielding

$$K_l = -[6/\tan^2(\alpha)](\ln[8\ell_g/H_t] - \ln[1 + 8\ell_g/H_t]), \quad (7)$$

TABLE I. Physical properties of the gases used in the experiments of Fig. 9(b) for $T_{g0} = 298.15$ K and $p_{g0} = 10^5$ Pa. Therefore, for arbitrary values of the gas temperature T_g and pressure p_g, $\lambda = \lambda_0(T_g/T_{g0})(p_{g0}/p_g)$ and $\rho_g = \rho_{g0}(T_{g0}/T_g)(p_g/p_{g0})$.

	λ_0 ($\times 10^{-9}$ m)	μ_g ($\times 10^5$ Pa s)	ρ_{g0} (kg m^{-3})
Helium	180	1.98	0.16
Air	65	1.85	1.18
Krypton	55	2.51	3.42
SF_6	39	1.53	6.04

here we will retain the complete expression of K_l given by (4), with $\ell_\mu = H_t\,\mu_g/\mu$ (see the supplementary material in [18] for details).

The vertical velocity at which the lamella is *initially* expelled, $V_v(T_e)$, can be deduced from the force balance projected in the vertical direction, $\rho\, H_t^2 \dot{V}_v \propto F_L = K_u\,\rho_g V_t^2 + K_l\,\mu_g\,V_t$, from which it can be deduced that

$$V_v(T_e) \propto \sqrt{F_L/(\rho H_t)}. \quad (8)$$

The splash criterion in [18] results from imposing that the vertical velocity (8) is such that $\beta = V_v/V_{TC}$, with $V_{TC} = \sqrt{2\sigma/\rho H_t}$ the capillary retraction velocity [35,36] and $\beta \simeq 0.14$.

Equation (4) reveals that the lift force exerted by the lubrication layer located beneath the advancing front depends logarithmically on the ratio λ/H_t, with λ the mean free path of the gas. It will be shown below that the ratio λ/H_t could be of order unity or even larger. This is the reason why the splash threshold velocity is sensitive to small changes of H_t. Motivated by this fact, and in order to account for the effect of the boundary layer developing upstream of the ejected liquid sheet, the equations for the ejection time (1) and for the thickness of the lamella, H_t, will be slightly changed with respect to the corresponding expressions derived in R&G.

II. INFLUENCE OF THE BOUNDARY LAYER ON THE EJECTION TIME

The large values of the Reynolds number characterizing the splashing of a droplet impacting against a wall suggest that we should describe the tangential deceleration of the fluid at the solid substrate by means of boundary-layer theory. As a first step, the results of the types of simulations describing the impact of a drop against a shear free wall described in [37] and illustrated in Figs. 2(a) and 2(b) provide the velocity field at the solid substrate for different instants of time: the radial velocity field computed using potential flow theory corresponds to the far-field boundary condition for the velocity component tangent to the solid, v_r, in the boundary-layer equations. Interestingly, Fig. 2(b) reveals that the stagnation-point type of flows used in previous studies [38–40] are in clear disagreement with the real ones. More precisely, Fig. 2(b) reveals that, in the neighborhood of the spatial region from which the lamella is ejected, $r = a(t) = \sqrt{3t}$, the computed radial velocity at $z = 0$ is much larger than the corresponding velocity corresponding to a stagnation-point type of flow,

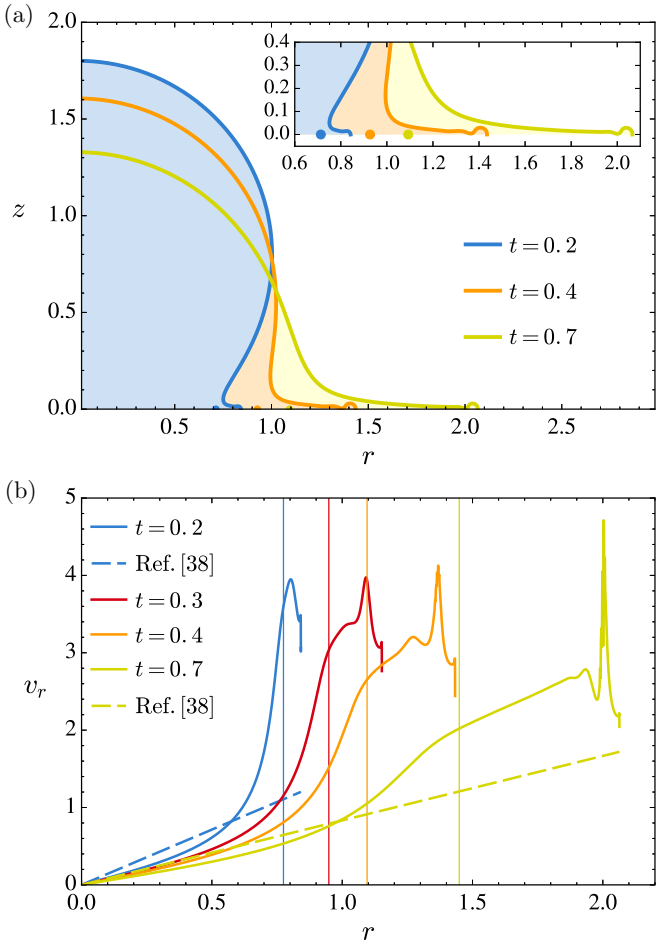

FIG. 2. (a) Computed shapes of a drop using the potential flow numerical code described in [37] for a value of the Weber number We = 100. The inset indicates the position of the stagnation point existing in the flow in a relative frame of reference translating with a velocity $\dot{a}$ for different instants of time. (b) Comparison between the computed values of the radial velocity $v_r(r,z=0)$ corresponding to the different drop shapes depicted in part (a) (continuous lines) and the radial velocity field assumed ad hoc in [38] (dashed lines). The origin $r = 0$ corresponds to the impact point. The vertical lines indicate the radial position of the root of the lamella, $r = a = \sqrt{3t}$.

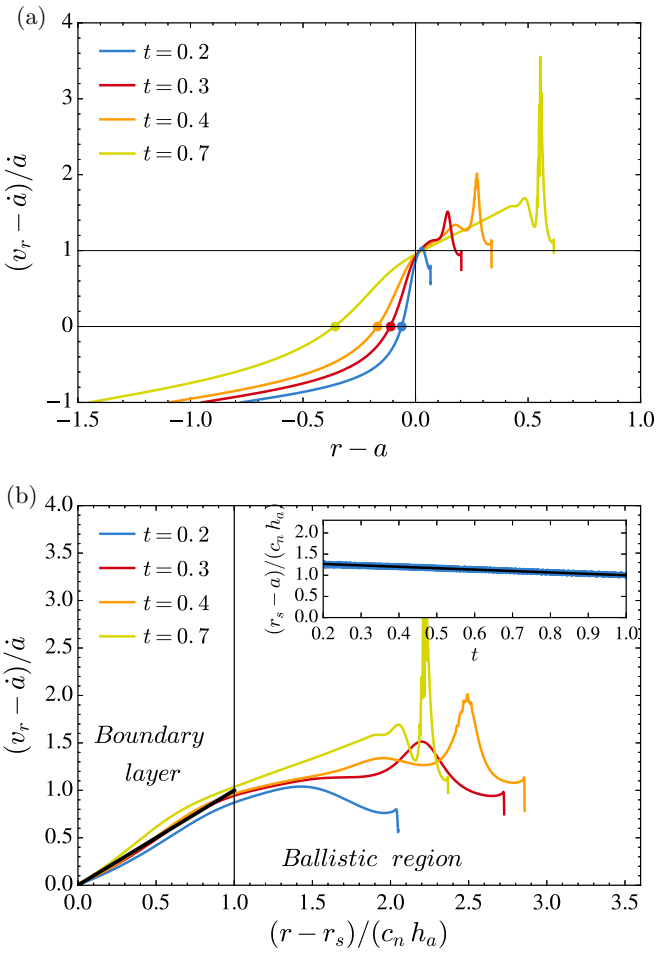

FIG. 3. (a) Time evolution of the values of the radial velocity profiles depicted in Fig. 2(b) represented in a frame of reference translating at a velocity $\dot{a} = 1/2\sqrt{3/t}$. The values of the radial velocity are normalized by $\dot{a}$ and are represented as a function of the distance to the root of the lamella, $r - a$. Notice that the relative radial velocity is $\dot{a}$ at $r = a$ and it is zero at $r = r_s$, with r_s indicating the radial position of the stagnation point in the relative frame of reference, marked using a colored dot. (b) The radial velocity v_r varies linearly between $r = r_s$ and $r = a$, namely the spatial region located between the stagnation point of the flow in the relative frame of reference and the root of the lamella. Indeed, notice that distances are normalized here by $r_s - a = c_n\, h_a(t)$, with $c_n = 1.5$ a constant (see the inset). The relevant region for the development of the boundary-layer flow entering into the lamella is $0 < (r - r_s)/(c_n\, h_a) < 1$, whereas the region $(r - r_s)/(c_n\, h_a) > 1$ corresponds to that of the ejected liquid sheet, which can be described using a ballistic approximation [37,42].

$v_r \approx r/t$. This analytical form of the radial velocity, $v_r \approx r/t$, is used, for instance, in Refs. [38–40]; it will also be shown below that the relevant outer velocity field for the development of the boundary-layer flow entering the ejected thin liquid sheet is not the one considered in [16,41] either.

Indeed, Fig. 3(a) represents the radial velocity field computed using potential flow simulations [37] in a frame of reference moving at $\dot{a}$, namely the speed at which the root of the lamella, located at $r = a$, propagates radially. Interestingly enough, Fig. 3(a) shows that, in agreement with potential flow theory [28,30–32] and by virtue of the Euler-Bernoulli equation applied in the moving frame of reference [18], the velocity entering into the lamella in the moving frame of reference is $\dot{a}$ *once the lamella is ejected*, i.e., the velocity of fluid particles entering into the lamella is $2\dot{a}$ in the fixed frame of reference. Figure 3(a) also indicates that fluid particles entering into the lamella come from a very narrow region, located between $r = r_s$ (which is the radial position of the stagnation point of the flow in the moving frame of reference) and the root of the lamella. Therefore, the relevant spatial region to describe the boundary-layer flow of interest here is the one located between $r_s < r < \sqrt{3t}$, where the radial velocity field computed using potential flow theory [37] notably differs from that assumed in previous studies [16,38–41], as will be shown below.

First, Fig. 3(b) shows that $\sqrt{3t} - r_s(t) = c_n h_a(t) \propto t^{3/2}$, with $c_n = 1.5$, a result that is consistent with Eq. (6) for the

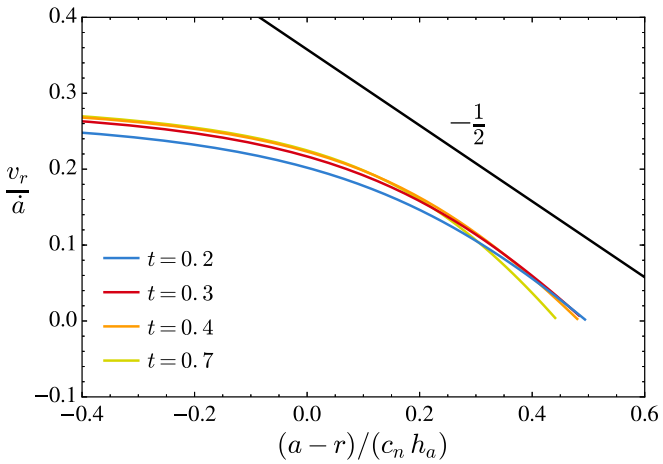

FIG. 4. Log-log plot of the radial velocity as a function of the distance to the root of the lamella. In agreement with Eq. (9), the radial velocity decays as $(a-r)^{-1/2}$ for $r \gtrsim r_s$.

velocity in the relative frame of reference provided in the supplementary material of [18],

$$\boldsymbol{v}_r - \dot{a}\,\boldsymbol{e}_x = -\frac{\sqrt{2a}}{\pi\sqrt{a-r}}[\sin(\theta/2)\mathbf{e}_r + \cos(\theta/2)\mathbf{e}_\theta] - \dot{a}\,\mathbf{e}_x, \tag{9}$$

from which it can be deduced that

$$(a-r_s)^{-1/2}\frac{\sqrt{2a}}{\pi} = \dot{a} \Rightarrow (a-r_s) = \frac{4}{\pi}\,h_a. \tag{10}$$

Figure 4 shows that, in agreement with Eq. (9), the radial velocity in the fixed frame of reference varies with the distance to the root of the lamella as $(a-r)^{-1/2}$ for $r \simeq r_s$. Even more interestingly, Fig. 3(b) shows that the radial velocity field for $r_s(t) < r < a(t)$ can be well approximated by

$$v_{\text{ext}} \simeq \dot{a}\left(1 + \frac{r-r_s}{c_n\, h_a}\right), \tag{11}$$

with $c_n = 1.5 \approx 4/\pi$; see Eq. (10). Due to the fact that in the spatial region $r_s < r < a$, $v_r/r \sim v_r/a$, and $\partial v_r/\partial r \sim v_r/h_a$, it can be deduced that, for $t \ll 1$, $v_r/r \ll \partial v_r/\partial r$ because $a(t) \gg h_a(t)$ ($a \propto t^{1/2}$ and $h_a \propto t^{3/2}$). Therefore, the continuity and momentum equations describing the radial and normal components of the velocity field within the boundary layer developing in the spatial region $r_s < r < a$ can be simplified to

$$\frac{\partial V_r}{\partial X} + \frac{\partial V_z}{\partial Z} = 0,$$
$$V_r\frac{\partial V_r}{\partial X} + V_z\frac{\partial V_r}{\partial Z} = V_{\text{ext}}\frac{dV_{\text{ext}}}{dX} + \nu\frac{\partial^2 V_r}{\partial Z^2}. \tag{12}$$

In Eq. (12), the variable $X = R(r-r_s)$ has been defined to describe the boundary-layer flow between $r_s = a - c_n h_a$ and $r = a = \sqrt{3t}$, $V_{\text{ext}} = V\dot{a}[1 + (r-r_s)/(c_n\, h_a)]$ is defined in Eq. (11), and the quasisteady Euler-Bernoulli equation has been used to compute the pressure gradient in the boundary-layer region. Indeed, the local acceleration term has been neglected in the system (12) due to the fact that the residence time T_r of fluid particles in the spatial region, $r_s < r < a$, is

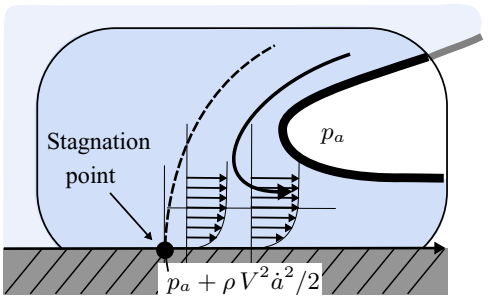

FIG. 5. Sketch of the flow developing between the stagnation point in the relative frame of reference and the root of the lamella.

$T_r \sim Rh_a/(V\dot{a}) \sim (R/V)t^2$, whereas the characteristic time of variation of the flow field in this region is $T_0 \sim (R/V)t$. Consequently, since the process of droplet splashing described here takes place for $t \ll 1$, and $O(\partial V_r/\partial T) \sim (V\dot{a})/T_0$ and $O(V_r\partial\, V_r/\partial X) \sim V^2\,\dot{a}^2/(R\,h_a)$, the order of magnitude of the ratio of the local and the convective acceleration terms in the momentum equation is $\sim T_r/T_0 \sim t \ll 1$, and thus the flow in the boundary-layer region, $r_s < r < a$, can be considered quasisteady.

In terms of the new dimensionless variables,

$$\bar{x} = \frac{X}{Rc_n\, h_a}, \quad \bar{z} = \frac{Z}{Rc_n\, h_a}\,(\text{Re}\, c_n)^{1/2}\,(\dot{a}h_a)^{1/2},$$
$$\bar{v}_r = \frac{V_r}{V\dot{a}}, \quad \bar{v}_z = \frac{V_z}{V\dot{a}}\,(\text{Re}\, c_n)^{1/2}(\dot{a}h_a)^{1/2}, \tag{13}$$

the system (12) reads

$$\frac{\partial \bar{v}_r}{\partial \bar{x}} + \frac{\partial \bar{v}_z}{\partial \bar{z}} = 0,$$
$$\bar{v}_r\frac{\partial \bar{v}_r}{\partial \bar{x}} + \bar{v}_z\frac{\partial \bar{v}_r}{\partial \bar{z}} = 1 + \bar{x} + \frac{\partial^2 \bar{v}_r}{\partial \bar{z}^2}. \tag{14}$$

The system (14) describes the growth of a boundary layer within an outer potential flow, which imposes a favorable pressure gradient: indeed, the pressure reaches a maximum at the stagnation point existing in the flow in the relative frame of reference, located at $r = r_s$, where $p = p_a + 1/2\rho\, V^2\dot{a}^2$, and pressure decreases downstream to match the atmospheric pressure, $p = p_a$, at the radial position from which the thin liquid sheet is ejected, $r \simeq a$; see Fig. 5.

The parabolic system of Eqs. (14), which needs to be solved subjected to the following boundary conditions:

$$\bar{x} = 0, \quad \bar{v}_r = \bar{v}_{r0}(\bar{z}),$$
$$\bar{z} = 0, \quad \bar{v}_r = 0, \tag{15}$$
$$\bar{z} \to \infty, \quad \bar{v}_r \to 1 + \bar{x},$$

admits a solution of the type

$$\bar{v}_r = (1+\bar{x})\frac{df}{d\bar{z}}(\bar{z}),\ \bar{v}_z = -f(\bar{z}), \tag{16}$$

with f given by the solution of the Falkner-Skan-type of equation [43],

$$\frac{d^3 f}{d\bar{z}^3} + 1 - \left(\frac{df}{d\bar{z}}\right)^2 + f\frac{d^2 f}{d\bar{z}^2} = 0, \tag{17}$$

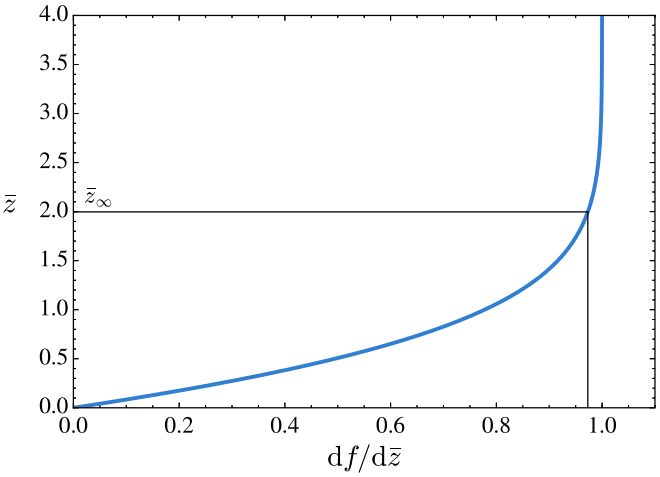

FIG. 6. Solution of Eq. (17) subjected to the boundary conditions given in Eq. (18).

satisfying the following boundary conditions:

$$f(0) = \left.\frac{df}{d\bar{z}}\right|_0 = 0 \quad \text{and} \quad \bar{z} \to \infty, \quad \frac{df}{d\bar{z}} \to 1. \tag{18}$$

Since the system of equations is parabolic, the downstream evolution of the velocity profiles loses memory of the initial condition at $\bar{x} = 0$, a fact favoring the solution convergence to that provided by Eq. (17) [44]. The solution of Eq. (17) subjected to the boundary conditions (18), which is represented in Fig. 6, reveals that the shear force per unit length F_τ exerted at the wall in the region $r_s < r < a$ and the thickness of the boundary layer δ are given, respectively, by

$$\begin{aligned} F_\tau &= \mu \int_0^{R(a-r_s)} \left.\frac{\partial V_r}{\partial Z}\right|_{Z=0} dX \\ &= \frac{3}{2} c_n^{1/2} \left.\frac{d^2 f}{d\bar{z}^2}\right|_0 \mu V \,\mathrm{Re}^{-1/2} \dot{a}(\dot{a}\, h_a)^{1/2} \\ &\simeq 1.1 \mu V \,\mathrm{Re}^{1/2}, \\ \frac{\delta}{R} &\simeq z_\infty\, c_n^{1/2} \left(\frac{h_a}{\dot{a}}\right)^{1/2} \mathrm{Re}^{-1/2} \\ &\simeq 2.45 \left(\frac{h_a}{\dot{a}}\right)^{1/2} \mathrm{Re}^{-1/2}, \end{aligned} \tag{19}$$

where use of the values $\bar{z}_\infty \simeq 2$ (see Fig. 6), $c_n^{1/2} = \sqrt{3/2}$, and $d^2 f/d\bar{z}^2(0) = 1.23 \approx \sqrt{3/2}$ has been made.

Making use of the estimation of the boundary-layer thickness in Eq. (19) and of Eq. (2), it can be concluded that, at the ejection time t_e,

$$\frac{\delta}{H_a} \simeq 4.34\,\mathrm{Re}^{-1/2}\, t_e^{-1/2}. \tag{20}$$

In the usual limit $\delta/H_a \ll 1$, the fluid within the ejected liquid sheet will be decelerated only by the action of interfacial tension forces. This assertion is true except in a very narrow region of thickness $\delta \ll H_a$ located near the wall, where viscous stresses also contribute to decelerate the liquid. Excluding the effect of this very thin region, the ejection condition $\dot{v}_t = \ddot{a}$ [18], with dv_t/dt the deceleration of the

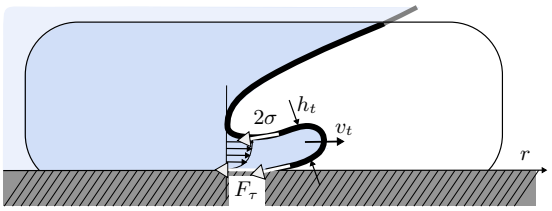

FIG. 7. Sketch of the forces decelerating the advancing front of the lamella.

edge of the lamella sketched in Fig. 7, reads

$$\rho H_a^2 \dot{V}_T \sim -2\sigma \Rightarrow \dot{v}_t \propto -\frac{\mathrm{We}^{-1}}{h_a^2}, \tag{21}$$

yielding the following expressions for both the ejection time and for the initial thickness of the lamella:

$$\begin{aligned} &\dot{v}_t \propto -\mathrm{We}^{-1}/h_a^2 \propto \ddot{a} \\ &\Rightarrow t_e \propto \mathrm{We}^{-2/3}, \quad h_a(t_e) \propto t_e^{3/2} \propto \mathrm{We}^{-1}. \end{aligned} \tag{22}$$

The scalings in (22), which have been verified numerically in [37], are valid only if

$$\begin{aligned} \frac{\delta}{H_a} &\simeq 4.34\,\mathrm{Re}^{-1/2}\, t_e^{-1/2} < 1 \\ \Rightarrow 4.34\,\mathrm{Re}^{-1/2}\,\mathrm{We}^{1/3} &= 4.34\,\mathrm{Re}^{1/6}\,\mathrm{Oh}^{2/3} < 1 \\ \Rightarrow \mathrm{Re}^{1/6}\,\mathrm{Oh}^{2/3} &\lesssim 0.25, \end{aligned} \tag{23}$$

where use of Eqs. (2), (20), and (22) has been made. In view of Eqs. (22) and (23), the ejection time is given by $t_e \propto \mathrm{We}^{-2/3}$ if $\mathrm{Re}^{1/6}\mathrm{Oh}^{2/3} < 0.25$. However, when the thickness of the boundary layer is similar to that of the lamella, namely $\mathrm{Re}^{1/6}\mathrm{Oh}^{2/3} \gtrsim 0.25$, fluid particles entering the ejected liquid sheet will also be decelerated by the action of the viscous shear force per unit length F_τ acting on a region of length $\sim H_a$, with F_τ calculated in Eq. (19) (see Fig. 7). Consequently,

$$\begin{aligned} \rho H_t^2 \dot{V}_T &\simeq -F_\tau - 2\sigma \\ &\simeq -\mu V\,\mathrm{Re}^{1/2}[1 + O(\mathrm{Re}^{-3/2}\,\mathrm{Oh}^{-2})] \\ &\simeq -\mu V\,\mathrm{Re}^{1/2} \\ \Rightarrow \dot{v}_t &\propto -\mathrm{Re}^{-1/2}/h_a^2. \end{aligned} \tag{24}$$

The final result expressed by Eq. (24) has been deduced neglecting the term $\mathrm{Re}^{-3/2}\,\mathrm{Oh}^{-2}$. This is done based on the fact that, in the regimes for which $\delta \sim H_a$, namely $\mathrm{Re}^{1/6}\mathrm{Oh}^{2/3} \gtrsim 0.25$, the Ohnesorge number satisfies the condition $\mathrm{Oh} \gtrsim 0.03$ (see Table II). Therefore, for the usual range of Reynolds numbers for which millimetric droplets splash, namely $\mathrm{Re} \sim 10^2 - 10^3$, $\mathrm{Re}^{-3/2}\,\mathrm{Oh}^{-2} < 1$. Finally, it can be concluded that the ejection time t_e in the regime $\mathrm{Re}^{1/6}\mathrm{Oh}^{2/3} \gtrsim 0.25$ can be calculated as

$$\begin{aligned} \dot{v}_t = \ddot{a} &\Rightarrow -\mathrm{Re}^{-1/2} \propto \ddot{a} h_a^2 \propto -t_e^{3/2} \\ &\Rightarrow t_e \propto \mathrm{Re}^{-1/3}. \end{aligned} \tag{25}$$

Figure 8 shows good agreement between the ejection times predicted by Eqs. (22) and (25) and the experimental ejection times reported in [18] and in [9]. Notice also that, while the ejection times predicted by Eq. (1) are also in good agreement with experiments for sufficiently low values of the Ohnesorge

TABLE II. Values of the material properties of the liquids, values of critical velocity for splashing V^*, values of the corresponding Reynolds numbers $\mathrm{Re} = \rho R V^*/\mu$ as well as the Ohnesorge numbers $\mathrm{Oh} = \sqrt{\mathrm{We}}/\mathrm{Re} = \mu/\sqrt{\rho R \sigma}$, and type of solid substrate: G, glass; P, parafilm; and S, steel, used to plot Fig. 9(a). (a) Acetone, (b) water, (c) methanol, (d) ethanol, (e) decamethyltetrasiloxane, (f) dodecamethylpentasiloxane, (g) poly(dimethylsiloxane), and (h) 10 cP silicone oil.

Ref.	Symb.	ρ (kg/m^3)	σ (mN/m)	μ (cP)	V^* (m/s)	Re ($-$)	Oh ($\times 10^3$)	Type
(a) [18]	●	789	24.0	0.3	3.12	7677	2.4	G
(b) [18]	●	1000	71.8	0.95	3.68	7583	2.5	G
[18]	♦	1000	71.8	0.95	3.70	6760	2.7	G
[18]	▶	1000	71.8	0.95	3.98	6832	2.8	G
[18]	●	1000	67.5	0.9	4.13	6395	2.9	G
(c) [18]	★	791	23.5	0.6	2.20	4507	3.5	G
[18]	★	791	23.5	0.6	2.74	3878	4.2	G
(d) [18]	■	789	22.6	1.0	1.77	2130	6.1	G
[18]	■	789	22.6	1.0	2.19	1834	7.3	G
(e) [18]	◀	854	17.2	1.3	1.56	1400	9.1	G
[18]	◀	854	17.2	1.3	1.71	988	11.4	G
(f) [18]	▼	875	17.8	1.7	1.55	1062	12.0	G
[18]	▼	875	17.8	1.7	1.81	830	14.7	G
(g) [18]	♦	913	18.6	4.6	1.77	466	30.5	G
[18]	♦	913	18.6	4.6	1.69	313	37.1	G
(h) [18]	▲	1000	19.5	10.0	1.95	258	62.2	G
[18]	▲	1000	19.5	10.0	2.02	182	75.3	G
[20]	●	989	56.4	1.23	3.83	3394	5.0	P
[20]	◀	982	48.1	1.50	3.54	2548	6.6	P
[20]	■	975	42.7	1.82	2.79	1492	8.9	P
[20]	♦	969	38.0	2.14	2.87	1233	11.5	P
[20]	▶	935	30.2	2.85	2.50	738	17.9	P
[20]	★	891	26.2	2.55	2.48	694	18.6	P
[20]	▲	843	23.8	1.88	2.34	840	14.8	P
[20]	▼	789	21.8	1.20	2.26	1186	10.2	P
[20]	●	989	56.4	1.23	4.68	4146	5.0	G
[20]	◀	982	48.1	1.50	3.81	2740	6.6	G
[20]	■	975	42.7	1.82	3.22	1724	8.9	G
[20]	♦	969	38.0	2.14	2.93	1259	11.5	G
[20]	▶	935	30.2	2.85	2.50	739	17.9	G
[20]	★	891	26.2	2.55	2.50	700	18.6	G
[20]	▲	843	23.8	1.88	2.38	855	14.8	G
[20]	▼	789	21.8	1.20	2.28	1198	10.2	G
[20]	●	989	56.4	1.23	4.08	3615	5.0	S
[20]	◀	982	48.1	1.50	3.98	2868	6.6	S
[20]	■	975	42.7	1.82	3.15	1689	8.9	S
[20]	♦	969	38.0	2.14	2.90	1246	11.5	S
[20]	▶	935	30.2	2.85	2.21	654	17.9	S
[20]	★	891	26.2	2.55	2.21	619	18.6	S
[20]	▲	843	23.8	1.88	2.18	783	14.8	S
[20]	▼	789	21.8	1.20	2.15	1127	10.2	S
[14]	●	786	20.5	2.0	1.51	738	14.1	G
[14]	◀	805	22.3	1.38	2.32	1045	11.7	G
[14]	■	805	22.3	1.38	1.68	1271	9.1	G
[14]	♦	1050	60.0	1.78	3.16	3096	5.5	G
[14]	▶	792	22.2	0.52	3.27	3893	4.4	G
[14]	★	792	22.2	0.52	2.50	4576	3.6	G
[14]	▲	1000	70.8	1.00	3.61	6479	2.8	G

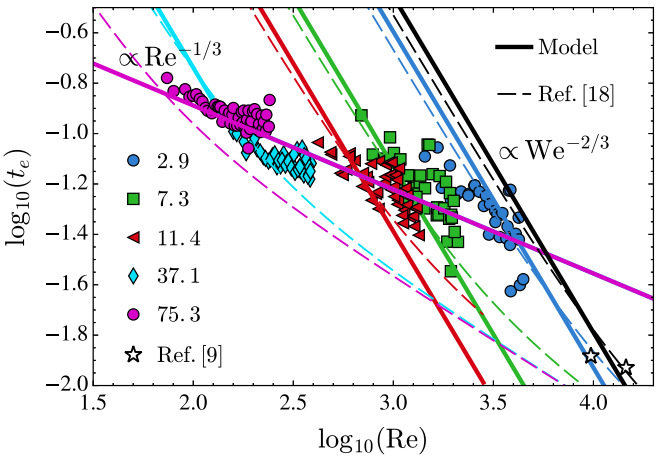

FIG. 8. Continuous lines represent the values of t_e calculated either as $t_e = 1.05\,\mathrm{We}^{-2/3}$ for $\mathrm{Re}^{1/6}\mathrm{Oh}^{2/3} < 0.25$ or as $t_e = 0.6\,\mathrm{Re}^{-1/3}$ for $\mathrm{Re}^{1/6}\,\mathrm{Oh}^{2/3} > 0.25$. Dashed lines represent the values of t_e obtained solving Eq. (1). The numerical values associated with each symbol represent $1000 \times \mathrm{Oh}$. The value of the Ohnesorge number is $\mathrm{Oh} = 2.3 \times 10^{-3}$ for the case of the experiments reported in [9].

number, the deviations between the predictions of Eq. (1) and measurements are apparent for the case of higher viscosity fluids.

The thickening of the lamella provoked by the development of a boundary layer between the stagnation point and the root of the ejected sheet can be approximately quantified imposing that the flow rate entering into the lamella coincides with that predicted by potential flow theory. Assuming a velocity profile within the boundary layer increasing linearly with the distance to the wall, the thickness of the root of the lamella, h_a^+, when the effect of the boundary layer is taken into account (see the sketch in Fig. 1) is given by

$$h_a v_a = v_a\left(h_a^+ - \frac{\delta}{R}\right) + \frac{\delta}{2R} v_a$$

$$\Rightarrow h_a^+ \simeq h_a(1 + 2.2/\sqrt{\mathrm{Re}\, t_e}), \tag{26}$$

with δ given in Eq. (19) and h_a given by Eq. (2). To improve the agreement with experiments for the smaller values of the Reynolds number, and due to the fact that, in the limit $\sqrt{\mathrm{Re}\, t_e} \gg 1$, the result in Eq. (26) can be very well approximated by

$$h_a^+ \simeq \frac{h_a}{1 - 2.2/\sqrt{\mathrm{Re}\, t_e}}, \tag{27}$$

we alternatively use here the following expression to calculate h_a^+:

$$h_a^+ = \frac{h_a}{1 - K_a/\sqrt{\mathrm{Re}\, t_e}}, \tag{28}$$

where K_a is a constant that will be determined by matching the predictions with the experimental data and whose precise value will be very close to our prediction in Eq. (27). In addition, to account for the thickening of the rim produced by the capillary retraction during the first instants after the ejection of the lamella (see the numerical shapes in Fig. 2 for illustrative purposes), the thickness of the edge of the advancing lamella

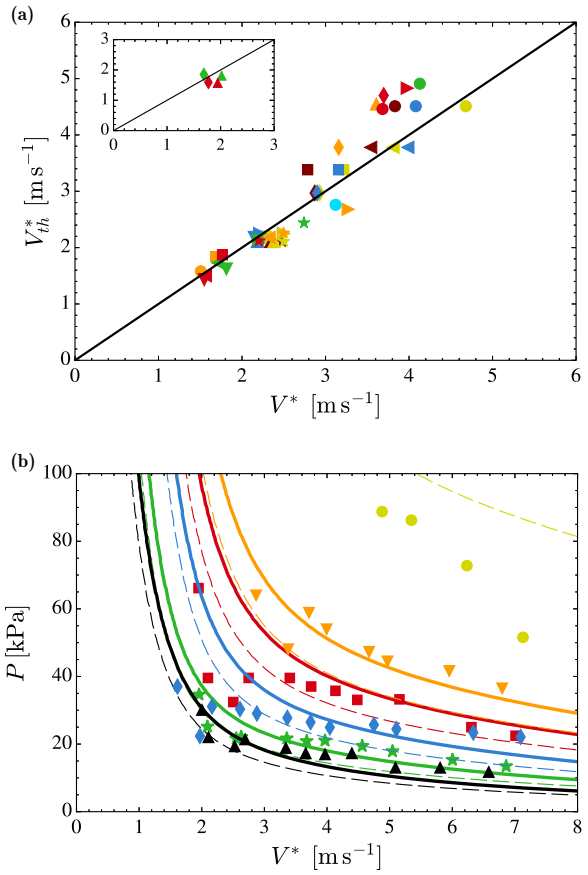

FIG. 9. (a) Comparison between the critical velocity V^* measured experimentally for the case $\mathrm{Re}^{1/6}\,\mathrm{Oh}^{2/3} < 0.25$ and the corresponding velocities predicted by Eq. (30). The material properties of the different liquids used, the type of solid substrate, the radii of the impacting drops, and the corresponding values of the Ohnesorge number are summarized in Table II. The inset represents the comparison between predicted and measured values of V^* when $\mathrm{Re}^{1/6}\,\mathrm{Oh}^{2/3} > 0.25$. In part (a), the surrounding gas is air at normal atmospheric conditions (see Table I). (b) Comparison between the predicted and measured values of the critical splash velocity for the case of the experiments reported in [4]. In this case, $\mathrm{Re}^{1/6}\,\mathrm{Oh}^{2/3} < 0.25$ and the material properties of the gases and liquids used are provided in Tables I and III, respectively. Continuous lines represent the predicted value of V^* for $K_h = 2$, while dashed lines represent the corresponding values of V^* for $K_h = 2.5$.

will be calculated here as

$$h_t = K_h h_a^+ = K_h \frac{h_a}{1 - K_a/\sqrt{\mathrm{Re}\, t_e}}, \tag{29}$$

a very similar expression to that suggested by the experiments in [18], where we found that $h_t \approx 2.8 h_a$.

Figure 9 shows a comparison between the experimental values of the splash threshold velocities satisfying the condition $\mathrm{Re}^{1/6}\mathrm{Oh}^{2/3} < 0.25$ and the theoretical ones, determined using

$$\left(\frac{F_L}{2\sigma}\right)^{1/2} = 0.14, \tag{30}$$

with F_L given by Eq. (3), t_e and h_t calculated through Eqs. (22) and (29), respectively, $\ell_\mu = H_t\,\mu_g/\mu$, $K_a = 2.8$, and the same values for the rest of the parameters as in [18]: $v_t = \sqrt{3}/2\, t_e^{-1/2}$, $\alpha = 61^\circ$, $K_h = 2.5$, and $H_0 = H_t/4$. The agreement between the predicted velocities and the experimental ones is fairly good in view of the wide range of viscosities, drop diameters, values of the interfacial tension coefficient, different substrate wettabilities [20], different gases, and different gas pressures considered [4], and this agreement can even be improved if the constant K_h is set to $K_h = 2$ in Fig. 9(b). The splash threshold velocities for the case $\mathrm{Re}^{1/6}\mathrm{Oh}^{2/3} > 0.25$, which are calculated in the same way as before, but making use of Eq. (25) to calculate t_e, are also in good agreement with the experimental data, as the inset in Fig. 9(a) shows.

TABLE III. Values of the material properties of the liquids used in [4], reproduced in Fig. 9(b), and values of the Ohnesorge numbers $\mathrm{Oh} = \sqrt{\mathrm{We}}/\mathrm{Re} = \mu/\sqrt{\rho R \sigma}$ corresponding to $R = 1.7$ mm. The material properties of the different gases used in the experiments reported in [4]—(a) helium, (b) air, (c) krypton, and (d) SF_6—are provided in Table I.

Gas		ρ (kg/m^3)	σ (mN/m)	μ (cP)	Oh ($\times 10^3$)	λ_0 (nm)	μ_g (cP)	ρ_{g0} (kg/m^3)
(a)	●	789	22.4	1.04	6.0	180	0.0198	0.16
(b)	■	789	22.4	1.04	6.0	65	0.0185	1.18
(c)	★	789	22.4	1.04	6.0	55	0.0251	3.42
(d)	▲	789	22.4	1.04	6.0	39	0.0153	6.04
(b)	▼	791	23.5	0.54	3.0	65	0.0185	1.18
(b)	◆	786	21.0	2.04	12.2	65	0.0185	1.18

Notice that, in the case of low viscosity liquids, and due to the fact that $t_e \propto \mathrm{We}^{-2/3}$ and since $h_t \sim t_e^{3/2} \propto \mathrm{We}^{-1}$, the height of the advancing liquid sheet can reach values close to the mean free path of gas molecules. Indeed,

$$\frac{\lambda}{H_t} \sim \frac{\lambda}{R}\,\mathrm{We} = \mathrm{We}_\lambda = \frac{p_{g0}}{p_g}\left(\frac{T_g}{T_{g0}}\right)\mathrm{We}_{\lambda 0}, \tag{31}$$

with $\mathrm{We}_\lambda = \rho\, V^2\, \lambda/\sigma$, and λ_0 is the mean free path at normal pressure and temperature conditions, p_{g0} and T_{g0}, respectively. For instance, in the case of helium in Fig. 9(b), $V^* \gtrsim 5\,\mathrm{m\,s^{-1}}$, $\sigma \simeq 20 \times 10^{-3}\,\mathrm{N\,m^{-1}}$, $\rho \simeq 780\,\mathrm{kg\,m^{-3}}$, $\lambda_0 \simeq 180 \times 10^{-9}$ m, and, therefore, $\mathrm{We}_\lambda \gtrsim 0.2$. This result suggests that calculations of the type reported in [45,46] are necessary to accurately predict the contribution of the gas lubrication layer to the lift force.

III. CONCLUDING REMARKS

The model developed in [18] has been completed by taking into account the effects associated with the growth of the boundary layer, which, when the velocity field is described in a moving frame of reference, develops between the stagnation point of the flow and the root of the ejected liquid sheet. Depending on the value of the ratio δ/H_t, with δ the thickness of the boundary layer and H_t the initial thickness of the advancing rim, the ejection time is calculated either as $t_e \simeq 1.05\,\mathrm{We}^{-2/3}$ if $\mathrm{Re}^{1/6}\mathrm{Oh}^{2/3} < 0.25$, or as $t_e \simeq 0.6\,\mathrm{Re}^{-1/3}$ if $\mathrm{Re}^{1/6}\mathrm{Oh}^{2/3} > 0.25$. Interestingly enough, the predictions for the ejection times for the larger values of the Ohnesorge number, $t_e \propto \mathrm{Re}^{-1/3}$, which contrast with $t_e \propto \mathrm{Re}^{-1/2}$ in [18], are in better agreement with the experimental measurements.

The predicted splash velocities are in fairly good agreement with experiments when both the modified ejection time and the thickening of the ejected lamella caused by the growth of the boundary layer are included in the splash criterion $(F_L/2\sigma)^{1/2} = 0.14$, deduced in [18].

ACKNOWLEDGMENTS

This work has been supported by the Spanish MINECO under Projects No. DPI2014-59292-C3-2-P and No. DPI2015-71901-REDT, and partly financed through European funds.

[1] C. Josserand and S. T. Thoroddsen, Annu. Rev. Fluid Mech. **48**, 365 (2016).
[2] S. Brodbeck, J. Police Sci. Pract. **2**, 51 (2012).
[3] Chr. Mundo, M. Sommerfeld, and C. Tropea, Int. J. Multiphase Flow **21**, 151 (1995).
[4] L. Xu, W. W. Zhang, and S. R. Nagel, Phys. Rev. Lett. **94**, 184505 (2005).
[5] S. Mandre, M. Mani, and M. P. Brenner, Phys. Rev. Lett. **102**, 134502 (2009).
[6] L. Duchemin and C. Josserand, Phys. Fluids **23**, 091701 (2011).
[7] J. M. Kolinski, S. M. Rubinstein, S. Mandre, M. P. Brenner, D. A. Weitz, and L. Mahadevan, Phys. Rev. Lett. **108**, 074503 (2012).
[8] S. T. Thoroddsen, T. G. Etoh, K. Takehara, N. Ootsuka, and Y. Hatsuki, J. Fluid Mech. **545**, 203 (2005).
[9] S. Thoroddsen, K. Takehara, and T. G. Etoh, J. Fluid Mech. **706**, 560 (2012).
[10] J. C. Bird, S. S. H. Tsai, and H. A. Stone, New J. Phys. **11**, 063017 (2009).
[11] R. Rioboo, M. Marengo, and C. Tropea, Exp. Fluids **33**, 112 (2002).
[12] A. Yarin, Annu. Rev. Fluid Mech. **38**, 159 (2006).
[13] C. W. Visser, P. H. Frommhold, S. Wildeman, R. Mettin, D. Lohse, and C. Sun, Soft Matter **11**, 1708 (2015).
[14] J. Palacios, J. Hernandez, P. Gomez, C. Zanzi, and J. Lopez, Exp. Therm. Fluid Sci. **44**, 571 (2013).
[15] C. S. Stevens, Europhys. Lett. **106**, 24001 (2014).
[16] J. Philippi, P. Y. Lagree, and A. Antkowiak, J. Fluid Mech. **795**, 96 (2016).
[17] C. J. Howland, A. Antkowiak, J. R. Castrejón-Pita, S. D. Howison, J. M. Oliver, R. W. Style, and A. A. Castrejón-Pita, Phys. Rev. Lett. **117**, 184502 (2016).
[18] G. Riboux and J. M. Gordillo, Phys. Rev. Lett. **113**, 024507 (2014).
[19] H. J. J. Staat, T. Tran, B. Geerdink, G. Riboux, C. Sun, J. M. Gordillo, and D. Lohse, J. Fluid Mech. **779**, R3 (2015).
[20] T. C. de Goede, K. G. de Bruin, and D. Bonn, arXiv:1701.02504.
[21] J. Hao and S. I. Green, Phys. Fluids **29**, 012103 (2017).
[22] S. Thoroddsen, J. Fluid Mech. **451**, 373 (2002).
[23] F. T. Smith, L. Li, and G. X. Wu, J. Fluid Mech. **482**, 291 (2003).
[24] C. Josserand and S. Zaleski, Phys. Fluids **15**, 1650 (2003).
[25] A. Korobkin, S. Ellis, and F. Smith, J. Fluid Mech. **611**, 365 (2008).
[26] P. D. Hicks and R. Purvis, J. Fluid Mech. **649**, 135 (2010).
[27] L. V. Zhang, J. Toole, K. Fezzaa, and R. D. Deegan, J. Fluid Mech. **703**, 402 (2012).
[28] Y. Scolan and A. Korobkin, J. Fluid Struct. **17**, 275 (2003).
[29] H. Wagner, Z. Angew. Math. Mech. **12**, 193 (1932).
[30] S. D. Howison, J. R. Ockendon, and S. K. Wilson, J. Fluid Mech. **222**, 215 (1991).
[31] S. Wilson, J. Eng. Math. **25**, 265 (1991).
[32] J. M. Oliver, Ph.D. thesis, Oxford University, 2002.
[33] P. D. Hicks and R. Purvis, J. Fluid Mech. **735**, 120 (2013).
[34] J. Maurer, P. Tabeling, P. Joseph, and H. Willaime, Phys. Fluids **15**, 2613 (2003).
[35] G. I. Taylor, Proc. R. Soc. London, Ser. A **253**, 296 (1959).
[36] F. E. C. Culick, J. Appl. Phys. **31**, 1128 (1960).
[37] G. Riboux and J. M. Gordillo, J. Fluid Mech. **803**, 516 (2016).
[38] I. V. Roisman, E. Berberović, and C. Tropea, Phys. Fluids **21**, 052103 (2009).
[39] I. V. Roisman, Phys. Fluids **21**, 052104 (2009).
[40] J. Eggers, M. Fontelos, C. Josserand, and S. Zaleski, Phys. Fluids **22**, 062101 (2010).
[41] S. Tabakova, F. Feuillebois, A. Mongruel, V. Daru, and St. Radev, Z. Angew. Math. Phys. **63**, 313 (2012).
[42] G. Riboux and J. M. Gordillo, J. Fluid Mech. **772**, 630 (2015).
[43] H. Schlichting, *Boundary-Layer Theory*, 7th ed. (McGraw-Hill, New York, 1975).
[44] K. K. Chen and P. A. Libby, J. Fluid Mech. **33**, 273 (1968).
[45] J. Li, Phys. Rev. Lett. **117**, 214502 (2016).
[46] J. E. Sprittles, Phys. Rev. Lett. **118**, 114502 (2017).